Electronic Supplementary Material (ESI) for CrystEngComm.

Supporting Information

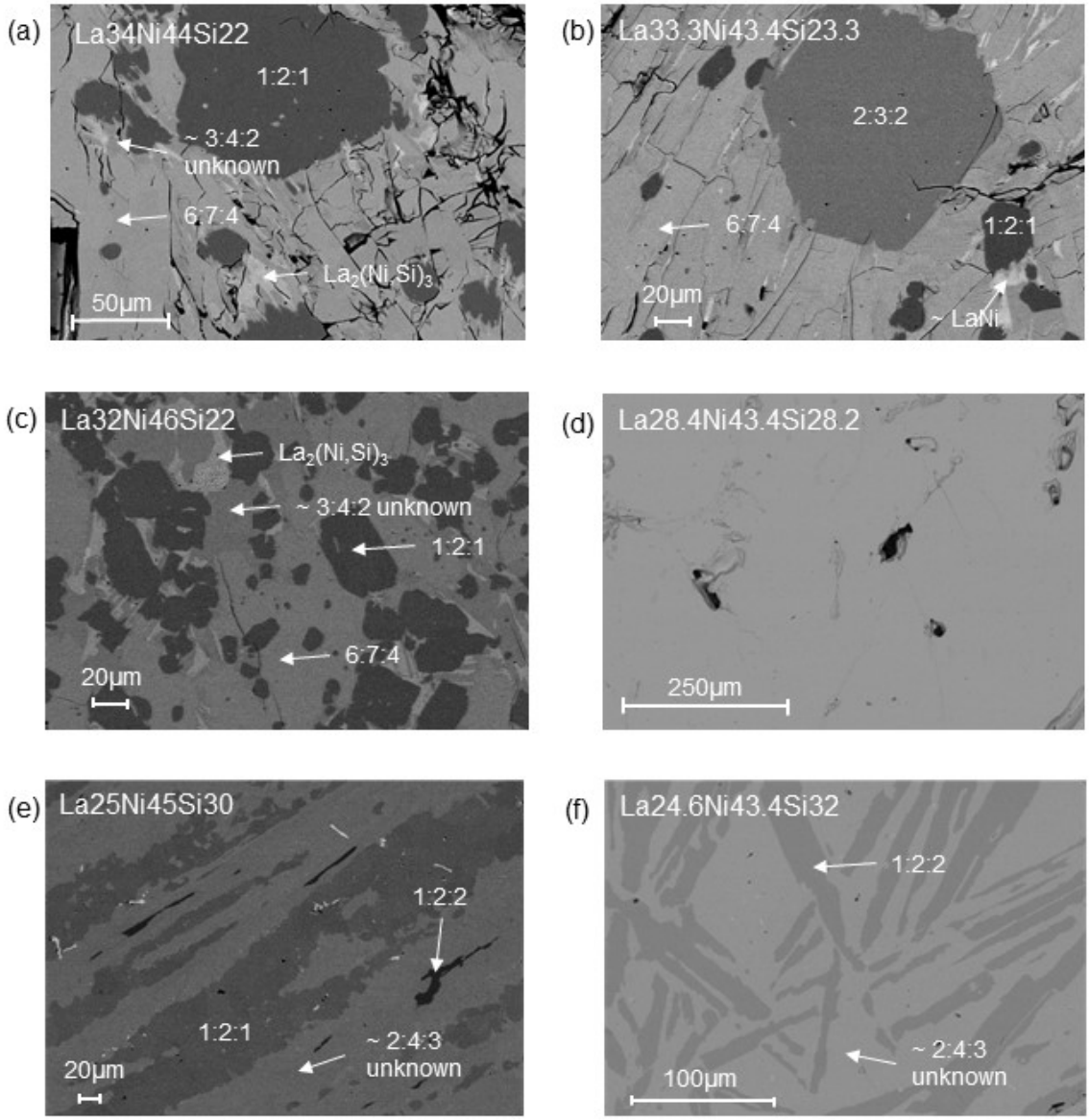

Figure S1. SEM images [backscattered electron (BSE) mode] showing the complex microstructure and multiphase appearance of samples. According to the numbering of Table 1, the nominal compositions are $La_{34}Ni_{44}Si_{22}$ [sample 3 (a)], $La_{33.3}Ni_{43.4}Si_{23.3}$ [sample 4 (b)], $La_{32}Ni_{46}Si_{22}$ [sample 5 (c)], $La_{28.4}Ni_{43.4}Si_{28.2}$ [sample 6 (d)], $La_{25}Ni_{45}Si_{30}$ [sample 8 (e)] and $La_{24.6}Ni_{43.4}Si_{32}$ [sample 9 (f)]. In each sample, the composition (La:Ni:Si at. %) of the different phases present is highlighted.

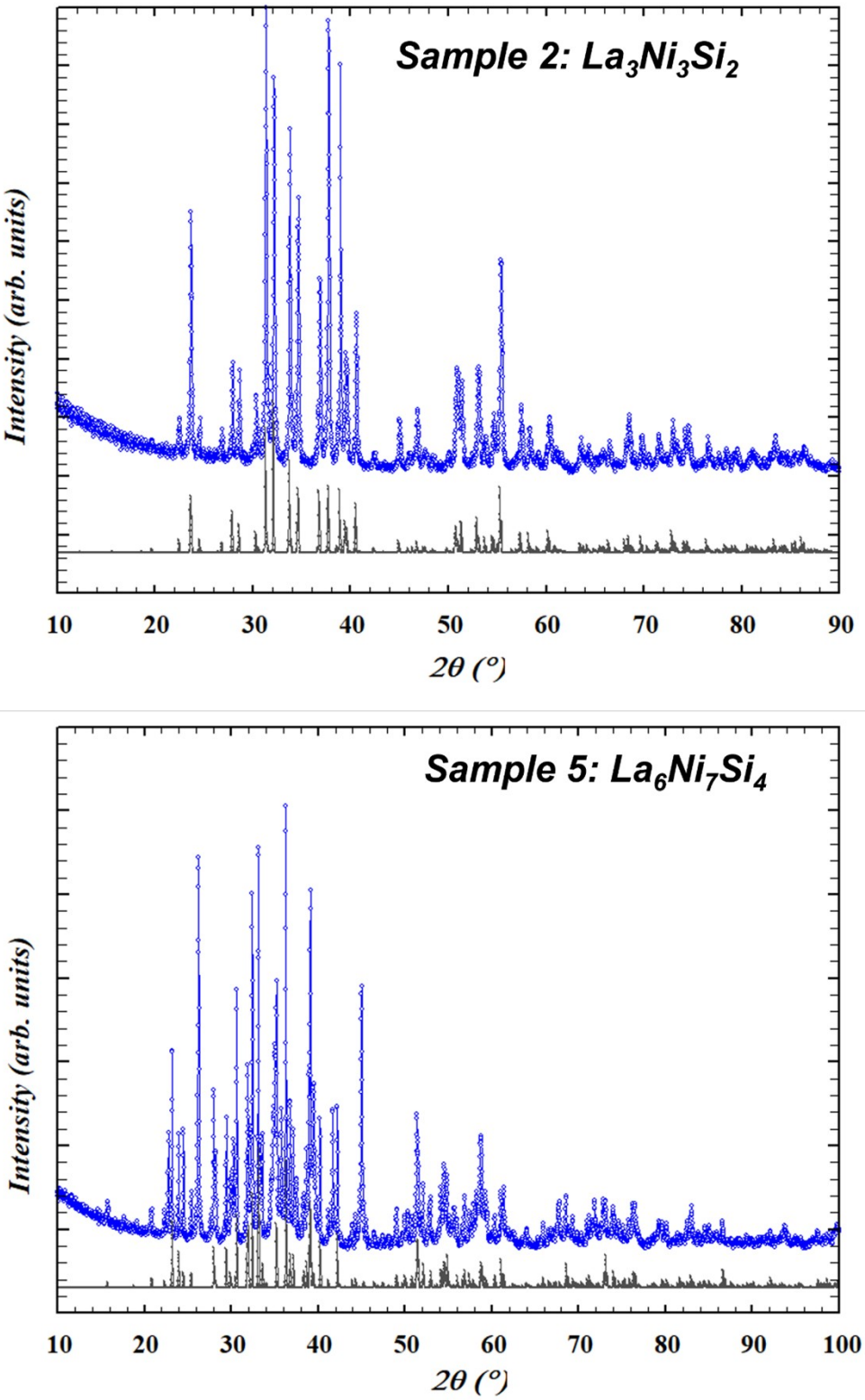

Figure S2. Top: powder pattern of sample 2 (nominal composition at. % La 37.5, Ni 37.5, Si 25.0), showing in blue and grey, respectively, the experimental and the calculated curves of the $La_3Ni_3Si_2$ compound. No additional phases are present. Bottom: powder pattern of sample **5**, having nominal composition $La_{32}Ni_{46}Si_{22}$ and containing the $La_6Ni_7Si_4$ compound as main phase; $LaNi_2Si$, ≈$La_3Ni_4Si_2$ (yet unknown) and $La_2(Ni,Si)_3$ are present as secondary phases. The simulated pattern of the main phase is reported for comparison.

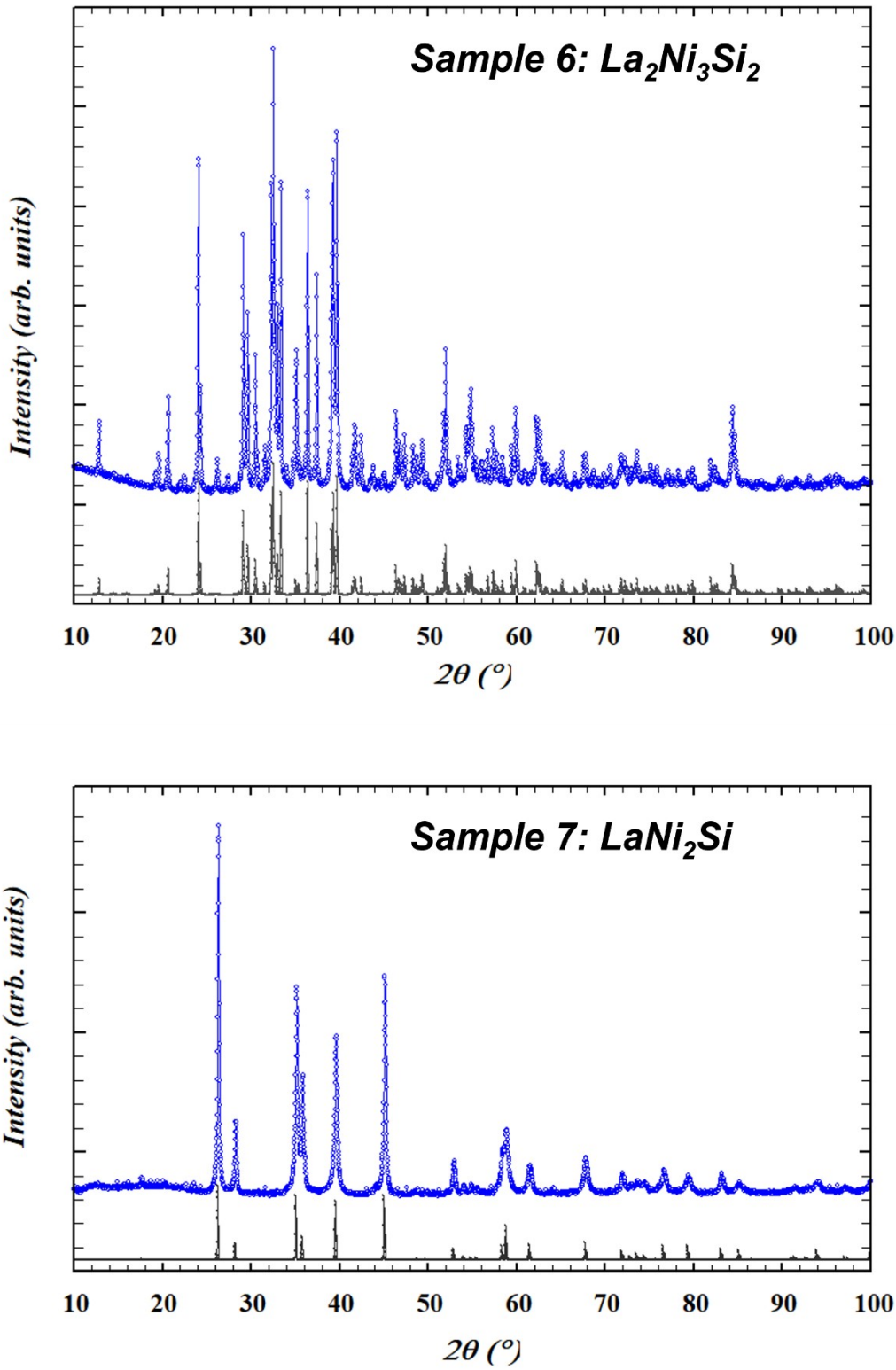

Figure S3. Top: powder pattern of sample **6** (nominal composition at. % La 28.4, Ni 43.4, Si 28.2), showing in blue and grey, respectively, the experimental and the calculated curves of the $La_2Ni_3Si_2$ compound. A few additional weak peaks are due to an impurity phase. Bottom: powder pattern of sample **7** (nominal composition at. % La 25, Ni 50, Si 25.0), almost single phase of the $LaNi_2Si$ compound; the simulated pattern is represented in grey.

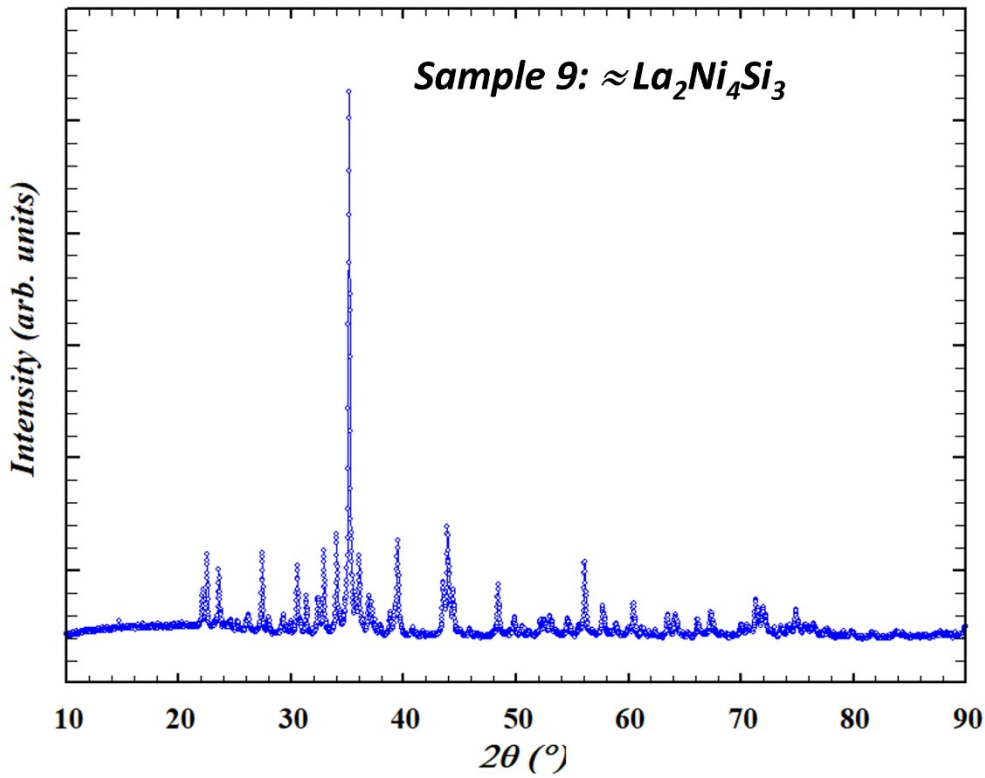

Figure S4. Powder pattern of sample **9** (nominal composition $La_{24.6}Ni_{43.4}Si_{32}$), containing the compound with approximate composition $La_2Ni_4Si_3$ (unknown structure), as predominant phase.

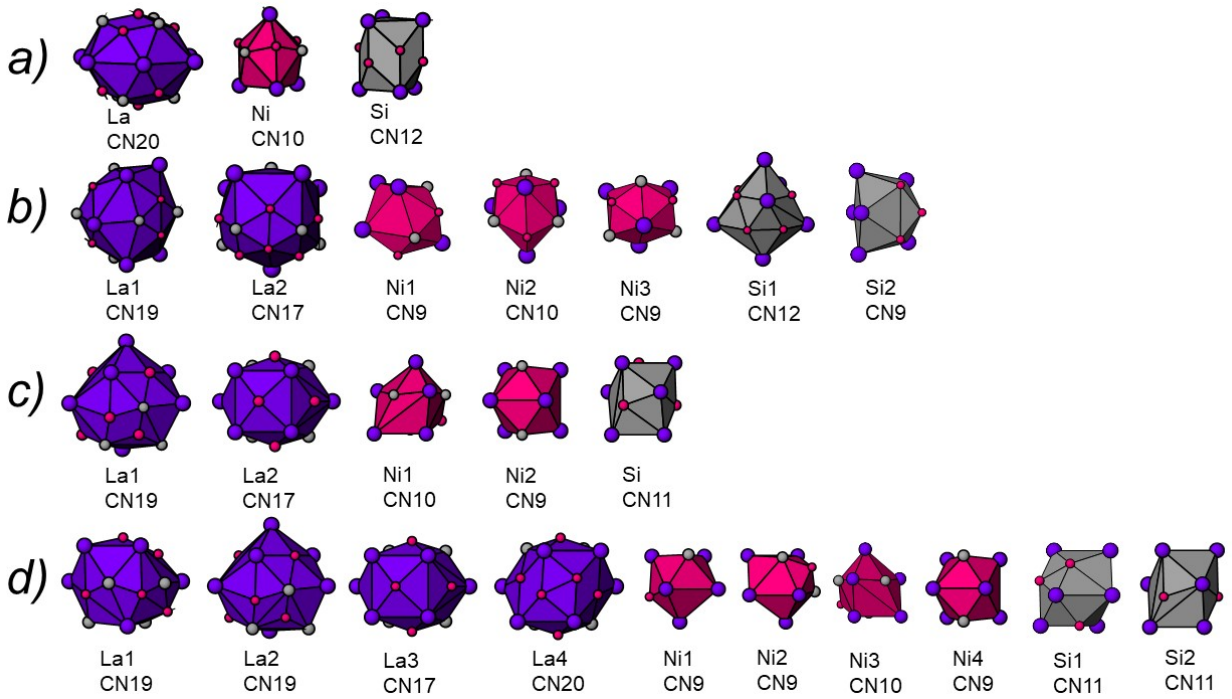

Figure S5. Coordination polyhedra in the crystal structures of $LaNi_2Si$ (a), $La_2Ni_3Si_2$ (b), $La_3Ni_3Si_2$ (c) and $La_6Ni_7Si_4$ (d). La, Ni and Si atoms are represented in violet, pink and grey, respectively.

Table S1. Details of the single crystal X-ray data collection and structure refinements of $LaNi_2Si$, $La_2Ni_3Si_2$, $La_6Ni_7Si_4$ and $La_3Ni_3Si_2$ (T = 295 K).

Compound	**$LaNi_2Si$**	**$La_2Ni_3Si_2$**	**$La_6Ni_7Si_4$**	**$La_3Ni_3Si_2$**
La:Ni:Si [composition in at.%]	25 : 50 : 25	28.6 : 42.8 : 28.6	35.3 : 41.2 : 23.5	37.5 : 37.5 : 25
Isotypic crystal	$SrCu_2Ga$	Own structure	$Pr_6Ni_7Si_4$	$Ce_3Rh_3Si_2$
Formula weight [g/mol]	284.42	510.13	1357.79	649.04
Crystal system	Rhombohedral	Monoclinic	Orthorhombic	Orthorhombic
Pearson symbol	*hR*12	*mP*28	*oP*68	*oP*32
Space group	$R\bar{3}m$ (No. 166)	$P2_1/c$ (No. 14)	*Pbcm* (No. 57)	*Pnma* (No. 62)
Unit formula per cell, *Z*	3	4	4	4
Lattice parameters [Å, °]	*a* = 4.0263(3) *c* = 15.066(2)	*a* = 6.8789(7) *b* = 6.2167(3) *c* = 12.214(1) β = 90.92(1)	*a* = 6.066(1) *b* = 7.488(1) *c* = 29.682(5)	*a* = 7.501(2) *b* = 14.316(4) *c* = 6.1485(16)
Unit cell volume [$Å^3$]	211.48(4)	522.24(9)	1348.2(4)	660.3(3)
Calc. density, ρ [g/cm^3]	6.70	6.49	6.68	6.53
Absorption coefficient, μ [mm^{-1}]	28.15	26.91	28.37	27.58
F(000)	381	904	2376	1132
Crystal shape	Elongated prism	Platelet	Block	Block
Crystal size [μm]	50 × 80 × 160	50 x 100 x 120	70 x 70 x 80	60 x 70 x 80
Scan mode	ω-ϑ	ω-ϑ	ω-ϑ	ω-ϑ
Theta range [°]	$2 \le \vartheta \le 32$	$2 \le \vartheta \le 30$	$2.5 \le \vartheta \le 33.5$	$3.6 \le \vartheta \le 31.4$
Ranges of *h*, *k*, *l*	$-6 \le h \le 6$ $-6 \le k \le 6$ $-22 \le l \le 22$	$0 \le h \le 9$ $-8 \le k \le 8$ $-17 \le l \le 17$	$-9 \le h \le 9$ $-11 \le k \le 11$ $-44 \le l \le 44$	$-10 \le h \le 10$ $-20 \le k \le 19$ $-8 \le l \le 8$
Number of collected reflections	970	3300	26857	6347
Number of independent reflections	116	1512	2503	1054
Reflections with $F_0 > 4\sigma(F_0)$	103	1080	1995	1044
Absorption correction method	ψ-scans, sphere	ψ-scans, sphere	multiscan	multiscan
Solution method	Patterson	Direct Methods	Intrinsic Phasing	Intrinsic Phasing
Number of refined parameters	9	65	81	41
R_1 [a]	0.012	0.032	0.029	0.022
wR_2 [b] (F_o^2), all data	0.034	0.064	0.053	0.055
R_{int} [c] (F_o^2)	0.059	0.044	0.046	0.040
Goodness-of-fit on F_o^2	1.273	0.920	0.923	1.249
Secondary extinction correction x	0.026(2)	0.0078(2)	–	0.0052(3)

[a] $R_1(F) = \left[\sum(|F_o| - |F_c|)\right] / \sum|F_o|$; [b] $wR_2(F^2) = \left[[\sum w(F_o^2 - F_c^2)^2] / [\sum w(F_o^2)^2]\right]^{\frac{1}{2}}$, w is a weight function different for each compound;

[c] $R_{int}(F_o^2) = \left[\sum\left|F_o^2 - \bar{F}_o^2\right|\right]/n$, is an internal agreement index quantifying the deviation of n equivalent intensities from the average value.

Table S2. Structure types adopted by lanthanide or alkaline earth ternary intermetallics with 1:2:1 stoichiometry: crystal data, number and representatives of each family.[2]

Structure Type	Pearson Code – Space Group	Wyckoff letters	Lattice Parameters [Å]	Number	Representatives
$BaLi_2Si$	*oP*8 – *Pmmn*	4*e*, 2*b*, 2*a*	*a* = 4.74 *b* = 6.75 *c* = 6.25	3	KLi_2As $BaNi_2Ge$
$PrCo_2Ga$	*oP*8 – *Pmma*	2 x 2*f*, 2*e*, 2*a*	*a* = 5.021 *b* = 4.043 *c* = 6.860	15	RCo_2Ga, R=La,Pr,Nd RCo_2In, R=Pr-Sm,Gd-Ho,Y RNi_2In, R=La,Pr,Nd $LaCo_{2.17}Zn_{0.83}$
$GdPt_2Sn$ (or $ZrPt_2Al$)	*hP*8 – $P6_3/mmc$	4*f*, 2*c*, 2*a*	*a* = 4.532 *c* = 9.065	29	RNi_2Sb, RPt_2Al, R=Zr,Hf RPd_2In, R=La, Ce RPt_2In, R=Ce,Gd,Tb-Ho,U RPt_2Sn, R=Gd,Tb,Er-Lu, Y,U UT_2Sn, T=Cu,Au RLi_2Ge, R=La,Ce $CaNi_2Si$, RNi_2Ge, R=Sr,Pr,Nd $LaCu_2Mg$, $MgAu_2Ga$
$CeLi_2Ge$ (or $AlCr_2C$ or $LiCu_2Sn$)	*hP*8 – $P6_3/mmc$	4*f*, 2*c*, 2*a*	*a* = 4.537 *c* = 7.568	4	RLi_2Ge, R=La-Nd
$SrCu_2Ga$	*hR*12 – $R\bar{3}m$	6*c*, 3*b*, 3*a*	*a* = 4.271 *c* = 15.925	3	$BaCu_2Ga$ $LaNi_2Si$
$CePt_2B$	*hP*12 – $P6_222$	6*i*,3*d*,3*c*	*a* = 5.4811 *c* = 7.8830	7	RPt_2B, R=La-Nd,Tm,Lu,Y
YPd_2Si (Fe_3C der.)	*oP*16 – *Pnma*	8*d*, 2 x 4*c*	*a* = 7.300 *b* = 6.927 *c* = 5.499	62	RPd_2Ga, R=La-Sm,Gd-Dy,Y RPd_2Si, RPd_2Ge, R=La-Lu,Y RNi_2Si, R=Tb,Dy,Er,Tm,Y RPt_2Si, R=Gd-Lu,Y $MgNi_2P$, UAu_2Al RPd_2Al, R=Ce-Pr $CaCd_2X$, X=Pd,Pt $CaMg_2X$, X=Rh,Pd,Pt
$EuAl_2Ge$	*oP*16 – *Pnma*	4 x 4*c*	*a* = 7.294 *b* = 4.306 *c* = 11.237	1	
$CeRh_2Si$ ($CeNiSi_2$-type occupation variant)	*oS*16 – *Cmcm*	4 x 4*c*	*a* = 4.0413 *b* = 17.730 *c* = 4.0675	3	RPt_2Si, R=Ce,Eu
YPd_2Sn ($MnCu_2Al$ Heusler phase)	*cF*16 – $Fm\text{-}\bar{3}m$	8*c*, 4*b*, 4*a*	*a* = 6.7144	~200	RMg_2Cu, R=Ce,Tb RMg_2Ag, R=La-Gd RMg_2Zn, R=Pr,Nd $LiCa_2X$, X=Tl,Si,Ge $MgNi_2X$, X=Sn,Sb $MgPd_2X$, X=Ga,Sb MgM_2In, M=Li,Ni,Pd $MgLi_2X$, X=Ga,In,Tl,Ge,Sn,Sb,Bi,Ag,Au,Zn,Cd,Hg ScM_2Ga, M=Ni,Pd,Cu ScM_2Al, M=Cu,Ag,Au,Ni,Pd,Pt ScM_2In, M=Ni,Pt ScM_2Sn, M=Pt,Rh $ScCo_2X$, X=Ga,Ge,Sn RPd_2In, R=Gd,Dy,Er-Lu,Sc,Y RM_2In, R= La-Lu,Sc,Y; M=Cu,Ag,Au RPd_2Tl, R=Sm-Er,Y RNi_2Sn, R=Yb,Lu,Sc RPd_2Sn, R=Gd-Lu,Sc,Y RPd_2Pb, R=Pr,Sm-Lu,Sc,Y RPd_2Sb, R=Gd-Er,Yb,Y RPd_2Bi, R=Pr,Sm-Er,Y RZn_2Mg, R=Ce,Tb
YRh_2Si ($CeNi_3$ der.)	*hP*24 – $P6_3/mmc$	12*k*, 4*f*, 2*d*, 2*c*, 2*b*, 2*a*	*a* = 5.495 *c* = 15.030	14	RCo_2Zn, R=La,Ce,Sm RNi_2Zn, R=La,Ce RRh_2Si, R=Er,Y; RRh_2Ge, R=Sm,Er,Y $SmCo_2Ga$, $LuNi_2Ga$, $TbFe_2Ga$
DyB_2C	*tP*32 – $P4_2/mbc$	8*g*, 3 x 8*h*	*a* = 6.791 *c* = 7.522	9	RB_2C, R=Tb-Lu,Sc,Y
$CeIr_2Si$	*tI*32 – $I4_1/amd$	3 x 8*e*, 4*b*, 4*a*	*a* = 4.0698 *c* = 35.408	4	RRh_2Si, RIr_2Si, R=La,Ce

Table S3. Atomic coordinates for the VASP optimizations based on the $CaNi_2Si$ structure (*hP*8).

Atom	Site	*x*	*y*	*z*
Ca/La	2*c*	⅓	⅔	¼
Ni	4*f*	⅓	⅔	0.96051
Si	2*a*	0	0	0

a = 4.004, c = 9.886 Å.